

Received October 29, 2020, accepted November 7, 2020, date of publication November 16, 2020, date of current version November 27, 2020.

Digital Object Identifier 10.1109/ACCESS.2020.3038168

Sensor Placement Optimization Based on an Improved Inertia and Adaptive Particle Swarm Algorithm During an Explosion

YONG-HONG DING^{1,2} AND WEN-BIN YOU¹

¹National Key Laboratory of Electronic Test Technology, North University of China, Taiyuan 030051, China

²School of Information and Communication Engineering, North University of China, Taiyuan 030051, China

Corresponding author: Yong-Hong Ding (303512944@qq.com)


This work was supported in part by the National Natural Science Foundation of China under Grant 61701445, and in part by the Open Research Fund of Key Laboratory of North University of China under Grant DXMBJJ2020-07.

ABSTRACT An explosion field is random and nonuniform, and test sensors can be damaged by fragments during blast wave monitoring. When accurately and comprehensively obtaining the experimental data and the dynamic distributions from an explosion field, the quantity and positioning of sensors during blast wave monitoring are important parameters. In this paper, an optimization method of sensor placement based on an improved inertia and adaptive particle swarm optimization (IIAPSO) algorithm is proposed to solve this problem. This work considers two new aspects: 1) the adaptive mutation mechanism and the inertia weight into classic particle swarm optimization (PSO) and 2) the propagation law of blast waves, the data errors and the probability of sensor damage during IIAPSO. These mechanisms are employed to enhance the global search ability and to increase data accuracy. First, the 12 benchmark functions are utilized to test the performance of the IIAPSO. The performance of the IIAPSO is compared with PSO, linear decreasing weighted particle swarm optimization (LDW-PSO) and adaptive particle swarm optimization (APSO) in terms of parameter accuracy and convergence speed. The results confirm that the proposed IIAPSO is more successful than PSO, LDW-PSO and APSO algorithms. Finally, the IIAPSO is used to optimize the sensor placement in an explosion field. The simulation and experimental results show that the feasibility of this algorithm is demonstrated.

INDEX TERMS Explosion field, sensor placement optimization, inertia and adaptive particle swarm algorithm, fitness function, damage uncertainty.

I. INTRODUCTION

In the development, production and use of weapon systems, blast damage effectiveness evaluation relies on comprehensive and accurate experimental data and a dynamic parameter distribution for the explosive field [1]–[4]. Explosion is a complex transient process accompanied by high temperature, high pressure and strong electromagnetic field [5], [6]. The random nonuniform rupture of a shell causes an anisotropic shock wave, and shock wave propagation will also be affected by the irregular reflection of the ground. So the extreme conditions in an explosion make the dynamic parameter measurements very challenging [4].

The associate editor coordinating the review of this manuscript and approving it for publication was Ravibabu Mulaveesala .

During a blast experiment, most of the sensor layouts in an air blast are circular around the TNT. A circular layout facilitates the reconstruction of the spatial blast waveform [4]. However, the experimental costs are high, and an improper sensor layout for blast wave monitoring can cause high coupling data, reducing the relevant characteristic value of the test data. In addition, sensors can be damaged by fragments during the test, and large errors can occur between the results of shock wave field reconstruction based on the limited test data and the actual results. Thus, it is vital to optimize the sensor layout in a shock wave field to save test costs and improve the experimental performance to reflect the overall blast wave generated by TNT.

Sensor layout optimization is a common problem in engineering tests. The initial research began in the field of aerospace. In 1991, Kammer [7] proposed a sensor

placement method that was based on ranking the contribution of each candidate sensor location to the linear independence of the corresponding target model partitions. In 2007, Lianzhen *et al.* [8] proposed a multi-object sensor placement optimization method in bridge health monitoring and structural model testing. In 2014, Liu *et al.* [9] presented a multi-objective fuzzy matter-element method to optimize the sensor quantity in a refrigerator car. Guo *et al.* [10] utilized travel time tomography with the subregion and multi-scale cell partition method to develop a method for optimizing sensor placement in uniform explosions. Bhushan *et al.* [11] and Farzin *et al.* [12] determined optimization problems based on the minimal cost requirements or sensor failures to achieve the desired reliability of the system. However, few studies have made progress in sensor placement optimization considering random, nonuniform and test sensor damage for blast wave monitoring.

Thus, it is necessary to develop a new sensor placement scheme in explosions for better shock wave measurement and reconstruction in the future. In this paper, a new method for sensor placement optimization in an explosion field is proposed that adopts an improved adaptive particle swarm algorithm (IIAPSO). The attenuation law of the shock wave in the propagation is applied to the criterion of data acquisition at the sensor placement. In addition, the data error and the probability of sensor damage are added into the fitness function so that the established fitness discriminant model established is consistent with the real test. This paper is organized as follows. The propagation law of the shock wave is introduced in Section II. The IIAPSO algorithm is proposed in Section III, the 12 benchmark functions are utilized to test the performance of the IIAPSO. The sensor placement optimization based on the IIAPSO algorithm is implemented in Section IV, and the numerical simulations and experimental test is used to test the feasibility of IIAPSO. Finally, we conclude this paper in Section V.

II. PROPAGATION LAW OF SHOCK WAVE

An ammunition explosion near the ground is equivalent to a semi-infinite space explosion, and the propagation law of the shock wave near the ground is similar to that in infinite space. The overpressure peak Δp can be obtained by formula (1) [13]–[15].

$$\Delta p = \begin{cases} \frac{0.076}{\bar{R}} + \frac{0.255}{\bar{R}^2} + \frac{0.65}{\bar{R}^3} & (1 < \bar{R} \leq 15) \\ \frac{1.07}{\bar{R}^3} - 0.1 & (\bar{R} \leq 1) \end{cases} \quad (1)$$

where $\bar{R} = \frac{r}{\sqrt[3]{\omega}}$ is the scaled distance, $m/kg^{1/3}$, r is the standoff distance of the place of measurement from the center of the explosion, and ω is the weight of the explosive in kilograms [16].

The shock wave propagates in the form of a sphere. The continuous diffusion during the propagation process will cause the positive pressure time of the shock wave to lengthen continuously. Meanwhile, the peak overpressure will rapidly

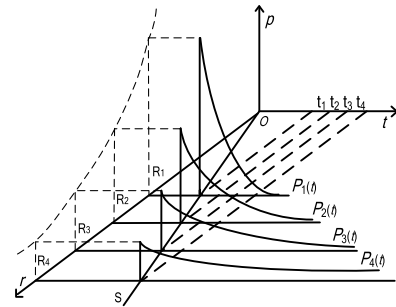


FIGURE 1. Blast overpressure-distance-time waveform.

decrease exponentially. The propagation law of shock wave overpressure with distance and time is shown in FIGURE 1.

$$p(t) = \Delta p \left(1 - \frac{t}{\tau}\right) e^{-\frac{\alpha t}{\tau}} \quad (2)$$

where τ is the positive pressure time,

$$\tau = \left(0.107 + 0.444\bar{R} + 0.264\bar{R}^2 - 0.129\bar{R}^3 + 0.0335\bar{R}^4\right) \cdot \sqrt[3]{\omega} \quad 0.05 \leq \bar{R} \leq 3 \quad (3)$$

α is the attenuation coefficient,

$$\alpha = \begin{cases} 0.5 + \Delta p & \Delta p \leq 0.1 \text{Mpa} \\ 0.5 + \Delta p \left(1.1 - (0.13 + 0.2\Delta p) \frac{t}{\tau}\right) & 0.1 \text{Mpa} < \Delta p \leq 0.3 \text{Mpa} \end{cases} \quad (4)$$

The propagation law is used as a constraint for subsequent shock field reconstruction.

III. IIAPSO ALGORITHM

A. CLASSIC PSO ALGORITHM

PSO is a global random search algorithm inspired by birds flocking in search of food [17]. In D -dimension space, the basic update formula of PSO of the d -th component of particle i is defined as follows [10], [18].

$$v_{id}(k+1) = wv_{id}(k) + c_1\xi(p_{best_{id}}(k) - x_{id}(k)) + c_2\eta(g_{best_d}(k) - x_{id}(k)) \quad (5)$$

$$x_{id}(k+1) = x_{id}(k) + v_{id}(k+1) \quad (6)$$

where v_i is the i -th particle velocity, x_i is the i -th particle position, p_{best} is the personal best position, g_{best} is the global best position, k is the number of iterations, and w is inertia weight, i.e., $0 < w < 1$; c_1 and c_2 are the learning factors, where c_1 is used to regulate the step size of particle to p_{best} and c_2 is used to regulate the step size of particle to g_{best} ; ξ and η are the random numbers with uniformly distribution in the range $[0, 1]$.

B. THE PROPOSED IIAPSO ALGORITHM

PSO is simple and easy to implement, but it is easy to be trapped in the local optimum and the convergence rate decreasing in the later period of evolution [19]–[21].

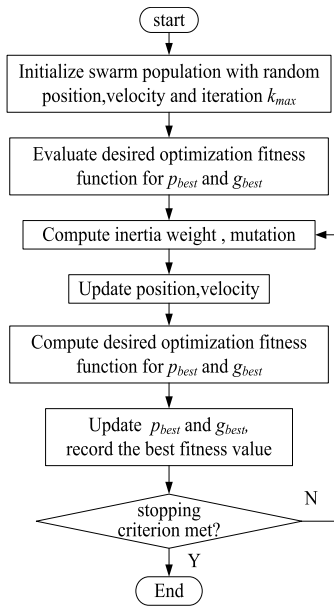


FIGURE 2. Flow chart of IIAPSO algorithm.

In this paper, an adaptive mutation mechanism and inertia weight were introduced to balance the local exploration and the global exploration and obtain the great advantages of the convergence property and avoid premature convergence.

In PSO, the initial population in an optimization problem may locate far away the real optimal solution, so in the proposed method, considering a variable step size $M(k)$ for mutation operator, it starts with a big mutation step size to increase the chance of searching new areas, and a small step size is used when the local solution reaches a near optimum solution. When a particle is selected to mutate, a Gaussian random disturbance is added to it as Equation (7) [21].

$$x'_{id}(k+1) = x_{id}(k+1) + M(k) \cdot \gamma \quad (7)$$

where γ is a random variable with a Gaussian distribution (mean is 0, variance is 1), $M(k)$ is a variable step size and defined as Equation (8).

$$M(k) = x_{\max} \cdot (\tanh(\text{fitness_}g_{\text{best}}/0.6)) \quad (8)$$

where x_{\max} is the maximum particle position, $\tanh(\cdot)$ is a hyperbolic tangent function, $\text{fitness_}g_{\text{best}}$ is the global best fitness.

In addition, to achieve better solution accuracy, the inertia weigh in Equation (5) is expressed as follows:

$$w = w_{\max} - \left(\frac{k}{k_{\max}}\right)^2 (w_{\max} - w_{\min}) \quad (9)$$

where w_{\max} and w_{\min} are the maximum and minimum inertia weights, and k_{\max} is the maximum number of iterations.

IIAPSO algorithm is used to find the best system parameter. The flow chart of IIAPSO algorithm is shown in FIGURE 2.

C. EVALUATION CRITERIA

① The mean fitness function [22] is the average of the fitness function value obtained from running the algorithm N times, as shown in Equation (10).

$$\text{MEAN} = \frac{1}{N} \sum_{k=1}^N x_k \quad (10)$$

where x_k is the best fitness value obtained at run k .

② The mean squared error (MSE) [21] is calculated by Equation (11).

$$\text{MSE} = \frac{1}{N} \sum_{k=1}^N e^2 = \frac{1}{N} \sum_{k=1}^N [x_k - \hat{x}_k]^2 \quad (11)$$

where x_k and \hat{x}_k are real and estimated values at run k , respectively.

③ Standard deviation (SD) [22] gives the variation of the fitness function value obtained from running the algorithm N times, as shown in Equation (12). It is an indicator of the stability and robustness of the algorithm.

$$\text{SD} = \sqrt{\frac{1}{N-1} \sum_{k=1}^N (x_k - \text{MEAN})^2} \quad (12)$$

D. SIMULATION COMPARISON OF IIAPSO AND DIFFERENT POPULAR PSO VARIANTS

To evaluate the performance of the IIAPSO algorithm, 12 benchmark functions (including Rastrigrin function, Sphere function and Ackley function, etc) are used to test PSO, linear decreasing weighted particle swarm optimization (LDW-PSO), adaptive particle swarm optimization (APSO) and IIAPSO algorithm. The functions are given by the TABLE 1.

The inertia weigh in LDW-PSO is expressed as follows:

$$w = w_{\max} - \frac{k}{k_{\max}} (w_{\max} - w_{\min}) \quad (13)$$

The inertia weigh in APSO is expressed as follows:

$$w = 0.5 (1 + \tanh(\text{fitness_}g_{\text{best}}/0.6)) \quad (14)$$

The tested dimensions were 30. Correspondingly, the maximum number of generations was set as 3000, and the population size was 20. For the experimental setting, 30 runs of the algorithm were performed; $c_1 = c_2 = 2$, $w = 1$ in PSO, $w_{\max} = 0.9$ and $w_{\min} = 0.4$ in LDW-PSO, APSO and IIAPSO.

The performance measurements for the 12 benchmark functions are listed in TABLE 2. The performance results are exhibited in terms of MEAN, MSE and SD. From the data in TABLE 2, it can be seen that the IIAPSO algorithm is superior to PSO, LDW-PSO and APSO in terms of optimization ability and stability.

TABLE 1. Test functions.

Functions	Function expressions	Space	Global minimum
Rastrigrin	$f_1(x) = \sum_{i=1}^D [x_i^2 - 10 \cos(2\pi x_i) + 10]$	[-5.12, 5.12]	0
Sphere	$f_2(x) = \sum_{i=1}^D x_i^2$	[-5.12, 5.12]	0
Ackley	$f_3(x) = -20 \exp\left(-0.2 \sqrt{\frac{1}{D} \sum_{i=1}^D x_i^2}\right) - \exp\left(\frac{i}{D} \sum_{i=1}^D \cos(2\pi x_i)\right) + 20 + e$	[-32, 32]	0
Rosenbrock	$f_4(x) = \sum_{i=1}^{D-1} [(1-x_i)^2 + 100(x_{i+1} - x_i^2)^2]$	[-5, 10]	0
Griewank	$f_5(x) = 1 + \frac{1}{4000} \sum_{i=1}^D x_i^2 - \prod_{i=1}^D \cos\left(\frac{x_i}{\sqrt{i}}\right)$	[-600, 600]	0
Alpine	$f_6(x) = \sum_{i=1}^D x_i \sin x_i + 0.1 x_i $	[-10, 10]	0
Schwefel's problem 22	$f_7(x) = \sum_{i=1}^D x_i + \prod_{i=1}^D x_i $	[-10, 10]	0
Rotated hyper-ellipsoid	$f_8(x_i) = \sum_{i=1}^D \sum_{j=1}^D x_j^2$	[-65.536, 65.536]	0
Step	$f_9(x_i) = \sum_{i=1}^D (x_i + 0.5)^2$	[-100, 100]	0
Levy	$f_{10}(x_i) = \sin^2(\pi \omega_i) + \sum_{i=1}^{D-1} (\omega_i - 1)^2 [1 + 10 \sin^2(\pi \omega_i + 1)] + (\omega_D - 1)^2 [1 + \sin^2(2\pi \omega_D)]$ where $\omega_i = 1 + \frac{x_i - 1}{4}$ ($i = 1, \dots, D$)	[-10, 10]	0
Rotated Ackley	$f_{11}(x) = -20 \exp\left(-0.2 \sqrt{\frac{1}{D} \sum_{i=1}^D x_i^2}\right) + \exp\left(\frac{i}{n} \sum_{i=1}^D \cos(2\pi x_i)\right) + 20 + e$, where $Y = M * X$	[-32, 32]	0
Rotated Griewank	$f_{12}(x) = 1 + \frac{1}{4000} \sum_{i=1}^D x_i^2 - \prod_{i=1}^D \cos\left(\frac{y_i}{\sqrt{i}}\right)$ $Y = M * X$	[-600, 600]	0

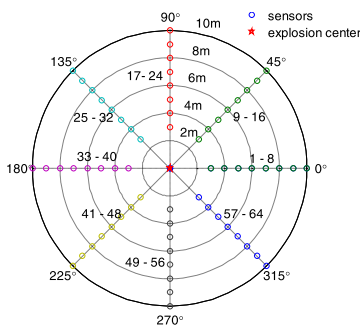


FIGURE 3. 64 sensor placement model.

IV. SENSOR PLACEMENT OPTIMIZATION BASED ON IIAPSO ALGORITHM

Ideally, the more sensors you have deployed, the more comprehensive the test data will be, assuming that 64 sensors are evenly distributed around the explosion center, as shown in FIGURE 3. The sensor position is expressed as $x(r, \theta)$ under polar coordinates. During an actual test, if \bar{R} is too large, the pressure is beyond the killing range; if \bar{R} is too small, the sensors are easily damaged. Therefore, the scaled distance \bar{R} is generally required to be 1~8, i.e., r varies (from 3 m to 10 m) away from the explosion center, and the angle between the adjacent radii is $\theta = 45^\circ$. The vertical distance between the explosion source and the ground is 1.5 m, and the TNT weighs 4 kg.

TABLE 2. Simulation results.

Function	Dimensions	Algorithm	MEAN	MSE	SD
Rastrigrin	30	PSO	4.472e+2	2.024e+5	4.969e+1
		LDW-PSO	1.484e+0	5.472e+0	1.839e+0
		APSO	3.841e+1	3.081e+3	4.076e+1
Sphere	30	IIAPSO	8.808e-3	9.821e-4	3.059e-2
		PSO	3.585e+02	1.330e+5	6.841e+01
		LDW-PSO	2.067e-1	2.620e-1	4.762e-1
Ackley	30	APSO	2.500e-3	7.058e-5	8.200e-3
		IIAPSO	1.202e-4	1.319e-7	3.613e-5
		PSO	1.995e+1	3.980e+2	6.53e-2
Rosenbrock	30	LDW-PSO	1.232e-1	2.262e-1	4.672e-1
		APSO	6.828e-3	2.054e-4	1.281e-2
		IIAPSO	5.787e-3	1.169e-4	9.286e-3
Griewank	30	PSO	9.528e+5	9.605e+11	2.333e+5
		LDW-PSO	1.940e-2	5.000e-3	6.920e-2
		APSO	2.958e-6	1.184e-10	1.065e-5
Schwefel's problem 22	30	IIAPSO	1.247e-6	2.532e-11	4.959e-6
		PSO	1.132e+3	1.318e+6	1.927e+2
		LDW-PSO	9.404e-1	1.051e+0	4.154e-1
Alpine	30	APSO	1.070e-2	1.677e-3	4.020e-2
		IIAPSO	7.825e-3	6.909e-4	2.552e-2
		PSO	7.512e+1	5.872e+3	1.539e+1
Levy	30	LDW-PSO	4.153e+0	3.822e+1	4.658e+0
		APSO	1.223e-1	4.390e-1	6.623e-1
		IIAPSO	4.300e-3	1.289e-4	1.070e-2
Rotated hyper-ellipsoid	30	PSO	8.615e+10	1.121e+23	3.290e+11
		LDW-PSO	9.480e-2	1.390e-2	7.140e-2
		APSO	9.970e+0	6.580e+2	2.403e+1
Rotated Ackley	30	IIAPSO	4.130e-2	5.000e-3	5.870e-2
		PSO	1.939e+6	3.837e+12	3.470e+5
		LDW-PSO	8.948e+0	4.920e+2	2.064e+1
Step	30	APSO	6.668e+2	1.333e+7	3.651e+3
		IIAPSO	5.56e-2	1.36e-2	1.043e-1
		PSO	1.269e+5	1.651e+10	2.049e+4
Levy	30	LDW-PSO	4.479e-1	8.118e-1	7.952e-1
		APSO	6.028e-4	7.683e-6	2.800e-3
		IIAPSO	6.944e-5	1.045e-7	3.211e-4
Rotated Griewank	30	PSO	6.716e+2	4.770e+5	1.638e+2
		LDW-PSO	1.686e-4	8.198e-8	2.354e-4
		APSO	7.303e-3	1.894e-6	1.200e-3
Rotated Ackley	30	IIAPSO	8.171e-5	4.002e-8	1.857e-4
		PSO	2.091e+1	4.371e+2	8.100e-2
		LDW-PSO	1.548e+1	3.169e+2	8.944e+0
Rotated Griewank	30	APSO	7.086e-1	1.467e+1	3.828e+0
		IIAPSO	9.000e-3	2.445e-4	1.300e-2
		PSO	1.153e+3	1.363e+6	1.835e+2
Rotated Griewank	30	LDW-PSO	9.738e-1	1.058e+0	3.364e-1
		APSO	1.810e-2	9.500e-3	9.740e-2
		IIAPSO	6.300e-3	5.426e-4	2.280e-2

Combined with the shock wave propagation law in terms of Equation (1)~(4) and the biharmonic spline surface interpolation algorithm (BSSIA) [15], the overpressure field model of the shock wave with 64 points is obtained, as shown in FIGURE 4.

The above IIAPSO algorithm is used to optimize the model.

A. FITNESS FUNCTION

A fitness function is used to evaluate the rationality of the optimized sensor layout.

During an actual test, due to the damage characteristics of ammunition, some test devices will be hit by fragments and lose data. At the same time, the data errors will be caused by obstacles or depressions in the propagation process of the shock wave. The data errors and the probability of device

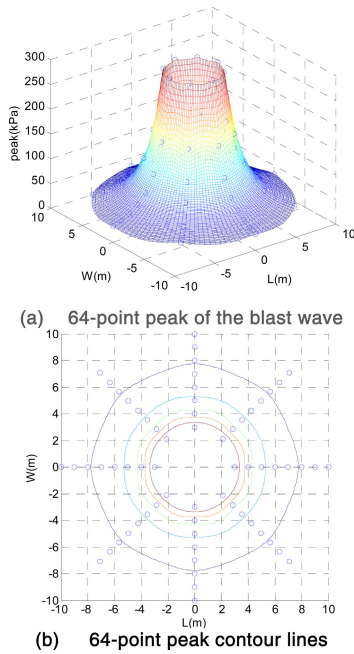


FIGURE 4. Overpressure field model constructed with 64 points.

damage are added into the fitness function to obtain the optimal IIAPSO solution.

Setting the quantity of sensors as n , p_{sn} is the interpolation pressure optimized by IIAPSO, and p_{64} is the interpolation pressure for 64 given ideal distributions. M is the number of interpolation data, and the uncertainty u_i can be expressed as

$$u_i = \sqrt{\sum_{j=1}^M \left(\frac{p_{sn}(x_j) - p_{64}(x_j)}{p_{64}(x_j)} \right)^2} / (M - 1) \quad (15)$$

The impact of shock wave vibration on the data uncertainty of the measuring point near the detonation center is greater for the fragmentation produced by the explosion of ammunition. The measurement uncertainty of testing points u_m is determined the distance of the detonation center, as shown in Equation (16).

$$u_m = \sqrt{\sum_{j=1}^n U_{mj}^2(x_j)} / (n - 1) \quad (16)$$

where n is the quantity of sensors, U_{mj} is the measurement uncertainty of a single point, it is close to linear distribution as shown in Equation(17).

$$U_{mj}(x_j) = ax_j + b \quad (17)$$

where a is the slope, b is the intercept. According to the statistics, $U_{mj} = 1\%$ at $r = 3$ m, the $U_{mj} = 0.5\%$ at $r = 10$ m, from which the coefficients of a and b can be obtained.

According to the statistical probability of the sensors being hit by fragmentation during a static detonation test over more than 20 years, the quantity and distribution of the fragmentation are different due to differences in the ammunition

and installation form, and the damage probability of sensors arranged at different test radii is nonlinear, which is related to the distance from the measuring point to the detonation center. Hence, the optimal sensor distribution can be obtained by maximizing the quantity of sensors arranged sensors n . The uncertainty u_d is

$$u_d = \sqrt{\sum_{j=1}^n U_{dj}^2(x_j)} / (n - 1) \quad (18)$$

where U_{dj} is the damage probability of the sensors.

There are many factors affecting the undetermined equations except for the above analysis, but the value by minimizing u_i , u_m and u_d can be used as a judging index with regard to optimizing sensor distribution.

It is hoped that the reconstruction shock wave field obtained by the optimized sensor distribution is as close as possible to the shock field reconstructed at 64 sensors, so the function of the optimization problem is

$$\begin{cases} \min f(x) = u_b = \sqrt{u_i^2 + u_m^2 + u_d^2} \\ \text{where } X = [x_{k1}, x_{k2}, \dots, x_{kn}] \\ \text{s.t. } x_{kj} \in I_{64} \end{cases} \quad (19)$$

The contribution of this paper is to use the IIAPSO algorithm to minimize the u_b so that the actual sensor placement in an explosion can be optimized for better reconstruction in the future.

B. OPTIMIZATION PROCESS BASED ON IIAPSO ALGORITHM

IIAPSO is used to obtain the optimal value of u_b and the sensor distribution. To make the sensor distribution meet the engineering requirements, the position x_i is calculated each time and rounded while searching for overlap points. If there are overlap points, one position is kept, and the rest are replaced with random integers. The detailed process is as follows:

Step 1. Produce a particle. The D -dimension particle is produced by selecting a distribution model randomly according to the quantity of sensors, which is expressed as $x = (r_1, r_2, \dots, r_n; \theta_1, \theta_2, \dots, \theta_n)$, where r_i and θ_i are the radius and angle of i -th sensor, respectively, and n is the quantity of sensors, where $D = 2n$.

Step 2. Initialize v_i and x_i for particle i . The position x_i is rounded, and overlap points are determined. If there are overlap points, keep one and replace the rest with random integers.

Step 3. Calculate the fitness function u_b and initialize p_{best} and g_{best} .

Step 4. Update the inertia weight, the variable step size, the particle velocity and position according to formulas (5)~(7) and calculate the fitness. The position x_i is rounded, and overlap points are determined. If there are overlap points, keep one and replace the rest with random integers.

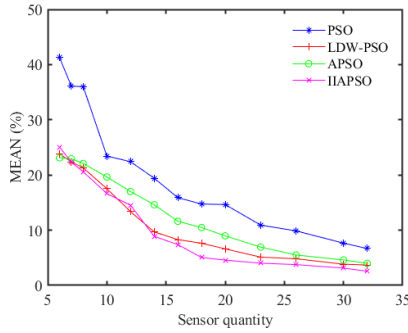


FIGURE 5. Simulation result by PSO, LDW-PSO, APSO and IIAPSO.

Step 5. Update p_{best} . The fitness value of each particle is compared with the fitness value of p_{best} , and p_{best} will be replaced if the former is better than latter.

Step 6. Update g_{best} . The fitness value of each particle is compared with the fitness value of g_{best} , and g_{best} will be replaced if the former is better than latter.

Step 7. Record the fitness value of g_{best} for each iteration.

Step 8. If the algorithm reach the maximum number of iterations, stop the operation and output the result; otherwise, return to Step 4.

C. NUMERICAL SIMULATIONS AND EXPERIMENTAL TEST

1) SIMULATION COMPARISON OF PSO, LDW-PSO, APSO AND IIAPSO

PSO, LDW-PSO, APSO and IIAPSO are applied to optimize the sensor distribution of FIGURE 3. The fitness function u_b is used to test the PSO, LDW-PSO, APSO and IIAPSO algorithms. For the experimental setting, each algorithm is run 30 times for each sensor distribution, the population size is 30, the max iteration number $t_{max} = 3000$, the inertia weight $w_{max} = 0.9$, $w_{min} = 0.4$, the particle velocity $v \in [-7, 7]$, and position $x \in [1, 64]$.

The MEANs of u_b for the different sensor quantities are shown in FIGURE 5 and TABLE 3. The results indicate that u_b obtained by PSO, LDW-PSO, APSO and IIAPSO decreases gradually with the increase of the sensor quantities, and the MEAN of u_b obtained by IIAPSO is superior to PSO, LDW-PSO and APSO when the sensor quantities is greater than 6. When the sensor quantities are greater than 18, the MEAN obtained by IIAPSO is less than 5%, but the change rate is significantly slower.

2) COMPARISON OF OPTIMIZED DISTRIBUTION AND TRADITIONAL SENSOR DISTRIBUTION

According to the military standard, 3~4 rays from the detonation center with a certain angle are used to lay the sensors, and each ray may lay 3~6 sensors. To compare the performance of the optimized sensor distribution, 20 sensor distributions are deployed in a ray distribution fashion with four angle positions (30°, 45°, 60°, 90°), as shown in FIGURE 6(a). According to TABLE 3, when the particle dimension $n = 20$, the MEAN value of u_b is 4.46%, and the sensor distribution optimized by IIAPSO is shown in FIGURE 6(b). The average

TABLE 3. Optimized results of PSO, LDW-PSO, APSO and IIAPSO.

Sensor quantities	MEAN by PSO(%)	MEAN by LDW-PSO(%)	MEAN by APSO(%)	MEAN by IIAPSO(%)
6	41.27	23.85	23.11	25.06
7	36.09	22.36	22.94	22.33
8	36.01	21.3	22.1	20.58
10	23.43	17.52	19.64	16.64
12	22.41	13.36	17.01	14.52
14	19.42	9.69	14.61	8.89
16	15.89	8.29	11.61	7.39
18	14.74	7.64	10.48	5.06
20	14.65	6.62	8.98	4.46
23	10.92	5.12	6.94	4.025
26	9.871	4.83	5.51	3.766
30	7.66	3.84	4.61	3.14
32	6.684	3.69	3.99	2.568

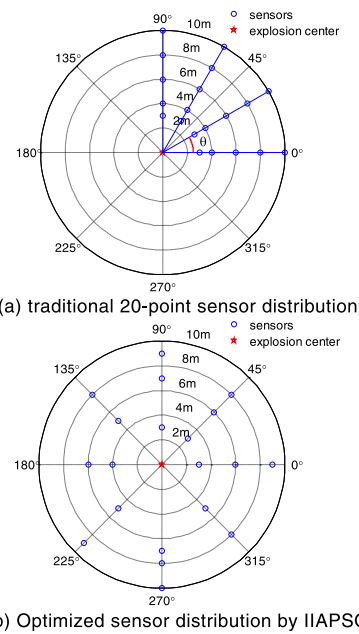


FIGURE 6. Different sensor distributions.

TABLE 4. Comparison of different sensor distributions.

Different distributions	Max errors (%)	Average errors (%)
$\theta=30^\circ$	404.78	103.23
$\theta=45^\circ$	309.06	68.99
$\theta=60^\circ$	207.74	40.08
$\theta=90^\circ$	37.16	10.38
Optimized distribution	13.03	4.46

errors and the maximum errors with the different sensors distributions are shown in TABLE 4. It is clear that the indexes in the optimized distribution are superior to those of the others.

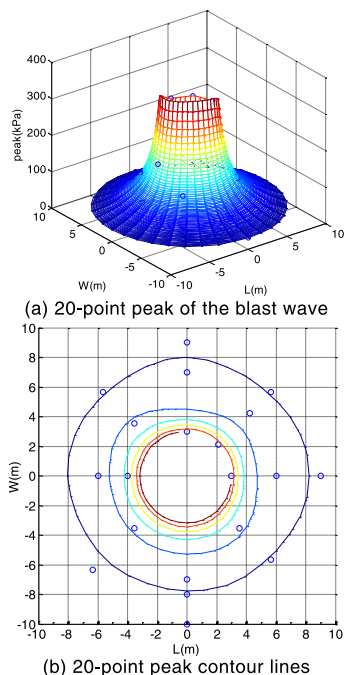


FIGURE 7. Overpressure field model constructed with 20 points.



FIGURE 8. Measured image.

The overpressure field reconstructed by the optimized distribution is shown in FIGURE 7. A comparison between FIGURE 7 and FIGURE 3 shows that the reconstructed peak distribution and peak contour lines based on the 20-point optimized sensor distribution are consistent with the 64-point distribution.

3) EXPERIMENTAL TEST

To further verify the optimization method, 20 shock wave recorders were installed in an explosion test according to FIGURE 6(b). The tested ground was concrete, the test recorders were installed in the center of a square steel plate with a side length of 400 mm and a thickness of 15 mm, and the radial parts of the measuring points were arranged on the steel plate with a 10 mm thickness. Then, 4 kg of cylindrical TNT was placed 1.5 m above the ground through a wooden frame, and a steel plate with a side length of 2 m and thickness of 10 mm was laid below the explosion center.

The test data from 20 measuring points are shown in TABLE 5. FIGURE 8 is the measured image. The overpressure field reconstructed by the 20 tested data points is shown in FIGURE 9(a), and the peak pressure contour lines are shown in FIGURE 9(b). It can be seen from FIGURE 8 that the wave front formed by the explosion is approximately

TABLE 5. Sensor distribution and test peak overpressure.

Number of test points	Angle (°)	Radius (m)	Δp obtained by experiment (kPa)
1	0	3	314.9
4	0	6	88.2
7	0	9	44.8
9	45	3	298.9
12	45	6	82.2
14	45	8	49.5
17	90	3	295.8
21	90	7	60.4
23	90	9	39.6
27	135	5	110.8
30	135	8	46.8
34	180	4	171.6
36	180	6	78.4
43	225	5	108.8
47	225	9	39.5
53	270	7	58.8
54	270	8	48.7
56	270	10	31.8
59	315	5	119.4
62	315	8	51.4

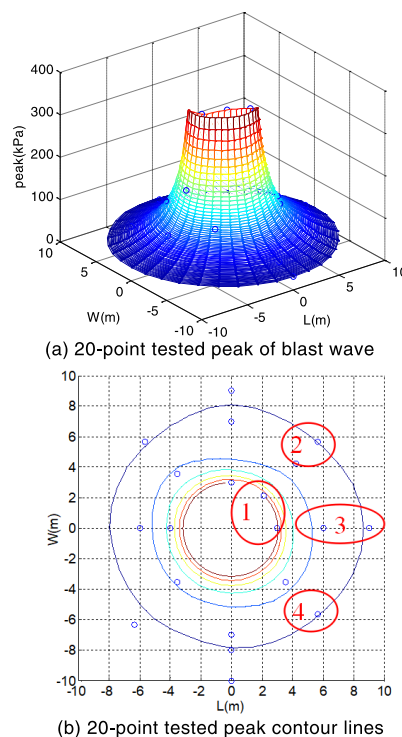


FIGURE 9. Tested overpressure field model with 20 points.

semi-spherical and slightly protruded outwards on the left side. As the blast wave velocity is proportional to the pressure, the peak pressure of this direction on the same scaled distance is greater than in other directions, which is consistent with the reconstructed peak pressure contour lines in FIGURE 9(b). The MEAN value of reconstruction between the tested data and the ideal 64-sensor distribution is 5.63%. It can be seen from FIGURE.7 and FIGURE.9 that they

are very similar, but in FIGURE.9(b), the contour line of the marked 1 is different from FIGURE.7(b). The distances between the contour lines marked 2, 3 and 4 and the sensors are different. The reasons for such similarity are as follows: ① Reasonable measurement points selected by IAPSO; ② The blast wave generated by the EXPLOSION of TNT cartridge without metal shell is evenly distributed in all directions; ③ The shock wave is less disturbed when it travels on the flat surface of cement and steel plate.

V. CONCLUSION

Shock wave tests are expensive and resources are limited, but the appropriate sensor number and placement are vital to obtain complete information on the shock wave field in the case of a certain damage probability, which can reduce measuring point data coupling. An optimization algorithm based on IAPSO is proposed for measuring the point optimization of a nonuniform explosion field. This paper shows that the u_b for different sensor distributions can be improved by the IAPSO algorithm. When the mean value of u_b is 4.46%, the quantity of sensors $n = 20$. The simulation and test results show that the reconstructed explosion field using the optimized data is consistent with an explosion image using 64 points, and the optimization algorithm is feasible.

ACKNOWLEDGMENT

The authors would like to express our thanks to the editor and anonymous reviewers for their help in revising the manuscript.

REFERENCES

- [1] Y. Wen-bin, M. Tie-hua, D. Yong-hong, C. Min, and Z. Jin-ye, "Dynamic modeling and application of shock wave testing system," *Chin. J. High Pressure Phys.*, vol. 4, no. 28, pp. 429–435, 2014.
- [2] P. Chunqiao, T. Gang, Z. Peijie, F. Qiang, L. Long, and Y. Shuqiang, "Effective method for predicting the parameters of shock waves in plateau environment," *J. Vibrat. Shock*, vol. 14, no. 37, pp. 221–226, 2018.
- [3] X. Hao, D. Hongmian, F. Jinbiao, Z. Jing, and W. Lingyu, "Research on low frequency characteristics and compensation method of a shock wave test system," *Explosion Shock Waves*, vol. 10, no. 39, 2019, Art. no. 104102.
- [4] S. Gao, G. Y. Tian, X. Dai, M. Fan, X. Shi, J. Zhu, and K. Li, "A novel distributed Linear-Spatial-Array sensing system based on multichannel LPWAN for large-scale blast wave monitoring," *IEEE Internet Things J.*, vol. 6, no. 6, pp. 9679–9688, Dec. 2019.
- [5] N. Jian-guo, W. Cheng, and M. Tian-bao, *Explosion and Shock Dynamics*. Beijing, China: National Defense Industry Press, 2010.
- [6] Y. Jia-Yan, *Research on Test Method of Ground Shock Wave in Near Earth Explosion*. Beijing, China: Nanjing Univ. Science & Technology, 2017.
- [7] D. C. Kammer, "Sensor placement for on-orbit modal identification and correlation of large space structures," *J. Guid., Control, Dyn.*, vol. 14, no. 2, pp. 251–259, Mar. 1991.
- [8] Z. Lian-zhen, H. Qiao, and W. Chao-hai, "Optimal sensor placement based on multi-object genetic algorithm," *Eng. Mech.*, vol. 24, no. 4, pp. 168–172, 2007.
- [9] L. Jing, Z. Xiaoshuan, X. Xinqing, and Z. Fu, "Optimal sensor layout in refrigerator car based on multi-objective fuzzy matter element method," *Trans. Chin. Soc. Agricult. Machinery*, vol. 45, no. 10, pp. 214–219, 2014.
- [10] G. Ya-Li, Y. Han, L. Wang, and L. Liu, "Sensor distribution design of travel time tomography in explosion," *Sensors*, vol. 7, no. 14, pp. 11207–11268, 2014.

- [11] M. Bhushan and R. Rengaswamy, "Comprehensive design of a sensor network for chemical plants based on various diagnosability and reliability Criteria. 2. Applications," *Ind. Eng. Chem. Res.*, vol. 41, no. 7, pp. 1840–1860, Apr. 2002.
- [12] F. Salehpour-Oskoue and M. Pourgol-Mohammad, "Fault diagnosis improvement using dynamic fault model in optimal sensor placement: A case study of steam turbine," *Qual. Rel. Eng. Int.*, vol. 33, no. 3, pp. 531–541, 2017, doi: 10.1002/qre.2031.
- [13] H. Zheng-Ping, *Explosion and Shock Measuring Technique*. Beijing, China: National Defense Industry Press, 2006.
- [14] Z. Jing, M. Tie-Hua, and F. Jin-Biao, *New Concept Dynamic Test*. Beijing, China: National Defense Industry Press, 2016.
- [15] Y. Wen-Bin, D. Yong-Hong, and Y. Yue, "Static explosion field reconstruction based on the improved biharmonic spline interpolation," *IEEE Sensors J.*, vol. 20, no. 13, pp. 7235–7240, Jul. 2020.
- [16] J. Kennedy and R. C. Eberhart, "Numerical and experimental analysis of the effect of different shapes of rigid barriers on blast wave propagation," in *Proc. 30th Int. Symp. Shock Waves*, G. Ben-Dor, O. Sadot, and O. Igra, Eds., 2017, pp. 721–724.
- [17] J. Kennedy and R. Eberhart, "Particle swarm optimization," in *Proc. Int. Conf. Neural Netw. (ICNN)*, Perth, WA, Australia, vol. 4, 1995, pp. 1942–1948, doi: 10.1109/ICNN.1995.488968.
- [18] X. zhan, Y. Cai, and P. He, "A three-dimensional point cloud registration based on entropy and particle swarm optimization," *Adv. Mech. Eng.*, vol. 12, no. 10, pp. 1–13, 2018.
- [19] M. A. Khanesar, M. Teshnehlab, and M. A. Shoorehdeli, "A novel binary particle swarm optimization," in *Proc. Medit. Conf. Control Autom.*, Jun. 2007, pp. 1–6.
- [20] Z.-L. Gaing, "A particle swarm optimization approach for optimum design of PID controller in AVR system," *IEEE Trans. Energy Convers.*, vol. 19, no. 2, pp. 384–391, Jun. 2004.
- [21] A. Alfi, "PSO with adaptive mutation and inertia weight and its application in parameter estimation of dynamic systems," *Acta Automatica Sinica*, vol. 37, no. 5, pp. 541–549, May 2011.
- [22] A. A. Nagra, "A study of hybrid particle swarm optimization and its applications," Ph.D. dissertation, Jiangsu Univ., Jiangsu, China, 2019.



YONG-HONG DING received the Ph.D. degree in measurement technology and instruments from the North University of China, Shanxi, Taiyuan, in 2014.

Since 2005, she has been working with the School of Information and Communication Engineering, North University of China. She is currently an Assistant Professor. She is the author of more than 30 articles and six patents. Her research interests include wireless communication

techniques, information processing, and dynamic testing. She received the honor of Sanjin Talents, in 2018.



WEN-BIN YOU received the Ph.D. degree in measurement technology and instruments from the North University of China, Shanxi, Taiyuan, in 2014.

He was a Visiting Scholar with the University of Pittsburgh, Pittsburgh, PA, USA, in 2016. He is currently an Assistant Professor with the School of Electrical and Control Engineering, North University of China. He is the author of more than 40 articles and more than ten patents. His research

interests include dynamic testing, calibration technology, and information processing.

...